A new simulation strategy for solid rocket motor ignition: coupling a CFD code with a one-dimensional boundary flame model, verification against a fully resolved approach

Laurent François, Joël Dupays, Marc Massot

A new simulation strategy for solid rocket motor ignition: coupling a CFD code with a 1D boundary flame model and verification against a fully resolved approach

Laurent François*
ONERA, 91123 Palaiseau, France

Joël Dupays†
ONERA, 91123 Palaiseau, France

Marc Massot‡
CMAP, CNRS, École polytechnique, Institut Polytechnique de Paris, 91128 Palaiseau, France

A new framework is presented for the simulation of ignition transients in complete solid rocket motors. The methodology is based on the coupling of a CFD solver for the combustion chamber flow field and a 1D solver for the unsteady combustion of the propellant, locally at each propellant boundary face of the CFD domain. Two approaches are presented. The first approach solves the propellant flame with a 1D approach, encapsulating all the numerical and multiscale modelling difficulties (surface processes, kinetics for the flame) within the boundary model. It enables a dynamic and physics-based transition from the initial inert heating of the propellant by the igniter flow to established burning, whereas traditional ignition models switch from an inert material behaviour to a quasi-steady empirical burning behaviour once a predefined ignition temperature has been reached, restricting the ability to reproduce fine ignition dynamics and unsteady combustion response. The second approach solves the propellant flame within the CFD domain, while only the surface and solid phase thermal profile are solved within the boundary model. While being more demanding in terms of mesh refinement, it allows for a detailed interaction between the ignition and the internal flow field to be obtained. Both approaches are compared for the laser-induced ignition of a propellant in one-dimension, and on a simplified yet demanding 2D test case where a propellant surface is impinged by a hot igniter jet flow. Despite the sensitivity of the configuration, the results compare very favourably, showing that accounting for the propellant flame only in the boundary model is acceptable and leads to accurate first ignition times. Yet, potential limitations and pitfalls of this approach are discussed, as well as subsequent improvements.

I. Introduction

Being able to accurately simulate the ignition transient of a solid rocket motor (SRM) is of paramount importance for the design of efficient and reliable propulsion systems. Since more than 50 years, various models and tools of increasing complexities have been developed to tackle this issue. Early volume-filling models [1, 2] failed at capturing the unsteady gas flow dynamics and progressive ignition of the propellant grain. Later 1D models improved those aspects [3, 4], however they could only capture more complex effects (ignition in complex geometries) via ad hoc corrections. Fully 3D models accounting for the true geometry of the combustion chamber have therefore emerged in the 1990s [5, 6] to enable an accurate reproduction of the internal flow dynamics (pressure waves, recirculations...). The 3D modelling involves the proper resolution of the conjugate heat transfer (CHT) at the propellant surface before ignition, a problematic that already involves many difficulties and is still the subject of a large research effort [7, 8]. Compared to the CHT framework, the solid propellant case adds multiple complexities: transition from an inert surface to a reactive surface, strong heat release from the propellant flame in a very thin zone above the propellant surface (typically a few hundred micrometers thick), parietal mass injection. The knowledge of the surface dynamics, propellant

*PhD student, DMPE, laurent.francois@onera.fr
†Research scientist, DMPE, joel.dupays@onera.fr
‡Professor, marc.massot@polytechnique.edu

flame chemistry and structure has progressed a lot but is still incomplete. Detailed CFD solvers (1D to 3D) are very computationally intensive [9–12] and cannot be considered for the simulation of a complete motor. In particular, the accurate capture of the propellant flame within the CFD domain would require very thin cells near the surface (typically 1μm), making the simulation of a complete motor ignition intractable in 3D.

Consequently, all the reported 3D approaches use a simplified modelling of the propellant ignition and combustion [13–15]; thus, we first present the state of the art in this field as well as analyse the stumbling blocks of such an approach The solid material, initially acting as an inert material, is heated up by convective and radiative heat fluxes from the gas phase. The unsteady evolution of the combustion chamber flow field is computed by a CFD solver. The thermal profile in the solid propellant is assumed one-dimensional locally at each boundary face and its unsteady evolution is coupled with the gas flow at regular intervals, allowing for a time-accurate simulation of the ignition transient. Once a propellant boundary face reaches a predefined ignition temperature, instantaneous ignition is assumed and the boundary model switches to a quasi-steady burning rate law (Vieille law) .

Several fundamental issues arise from the classical simplified modelling, which we list below:

1) The ignition temperature criterion is approximate and cannot easily account for the dependence of this temperature on pressure, heat flux history and level or other factors.
2) The instantaneous ignition, i.e. transition from inert heating to quasi-steady burning, automatically discards dynamic burning effects where the burn rate temporarily exceeds its steady-state value due to excessive pre-heating.
3) The propellant flame (be it explicitly modelled with analytical transient models [16], or conceptually hidden in semi-empirical burn rate laws) has a size on the order of 100 μm which means that it may well overlap with the first cells of the chamber CFD mesh. Thus potential interactions between the internal flow field and the flame may not be properly captured, e.g. erosive burning can only be included by empirically deduced correction factors. Additionally, the flame is assumed one-dimensional, thus potential lateral thermal expansion is not accounted for.
4) All the combustion models for large-scale ignition simulations use a quasi-steady propellant flame. As such, transient flame dynamics (flame establishment) may be inaccurate, in particular if the flame development time is not small compared to the characteristic time of ignition. Also propellant response to pressure oscillations will only be accurate at low frequencies for which the propellant (solid phase thermal profile and gas flame) may be considered quasi-steady.
5) No study has been presented to investigate the dependence of the computed ignition dynamics on the mesh refinement, in particular for the accuracy of the wall heat transfer and the propagation of ignition.

Some investigations at ONERA and collaborators [16–18] have included analytical transient flame models that enable a truly dynamic ignition to occur without relying on a temperature criterion, while also allowing dynamic burning effects. Still, these ignition models are largely simplified and require fine-tuning to better reproduce experimental results.

In the present work, we introduce two ignition models that offer a more detailed modelling of the ignition transient and of the propellant combustion. These models will enable to gain a deeper understanding of the previously mentioned effects.

The first model uses a refined mesh in the CFD domain and capture the propellant flame entirely within the CFD solver, avoiding the previous assumption of one-dimensionality for the flame. A one-dimensional model of solid propellant thermal profile and surface processes is used as boundary model. This detailed coupled model allows for an accurate depiction of the formation of the propellant flame and its interaction with the combustion chamber flow field. This approach is intractable for large-scale 3D simulations, however 2D simulations are possible.

The second model, inspired by the previous ignition models from ONERA [16, 18], constitutes a major step forward, relying on a previous in-depth study of mathematical models and numerical methods for the one-dimensional solid propellant combustion [19, 20]. A one-dimensional solid propellant combustion tool, including propellant flame dynamics, has been developed [20] and is introduced as a dynamic boundary model in the CFD solver CHARME from the multiphysics suite CEDRE from ONERA [21]. At each propellant boundary face of the CFD mesh, this model is fed with the corresponding wall heat flux evaluated by the CFD solver, and computes the unsteady evolution of the temperature profile inside the solid propellant, as well as the gradual development of the one-dimensional propellant flame. Compared to the previous transient flame models from ONERA, the gas phase combustion is solved numerically and can include detailed combustion kinetics if required, thus enabling more accurate combustion characteristics to be simulated. Ignition occurs dynamically as the flame appears in the 1D gas phase. The combustion products are injected in the CFD domain at the propellant surface, similarly to the other 3D ignition works already discussed.

Both coupled approaches are confronted on two cases using simplified kinetics: solid propellant laser-induced ignition in one-dimension, and a discriminating 2D case with impingement of a hot igniter jet flow on a propellant

surface, involving strong interactions between the flow field and the surface dynamics. The two approaches compare very favourably, in particular heating and first ignition time are virtually identical. This indicates that the boundary model involving a 1D flame does not induce physical artefacts due to the additional modelling assumptions it involves.

Still, specific modelling and numerical difficulties may appear when using this boundary model. Numerical experiments indicate that even if the new approach allows for a coarsening of the mesh near the surface, while still predicting properly the first ignition time and flame establishment, a larger coarsening leads to degraded dynamics in this sensitive configuration. We thus discuss in detail possible improvements and show that the proposed approach has a lot of potential for realistic configurations.

II. Modelling

In this section, we first present the detailed modelling of the propellant combustion, where the propellant flame and the combustion chamber flow field are captured within a single fluid model. We then introduce a one-dimensional flame as an additional sub-model to decrease the fluid model complexity.

A. Detailed model

The propellant combustion process, the chamber internal flow field and the conjugate heat transfer at the propellant surface can be represented by two models: one fluid model for the flow field (including gas phase reactions) and one for the evolution of the thermal profile inside the solid propellant. Both models are connected at the propellant surface via various balance equations, involving surface degradation of the solid. Let us present each model in detail, as well as the connection conditions.

1. Fluid model

The combustion chamber gas flow is modelled by the multispecies compressible Navier-Stokes equations. To improve the reproduction of the flow particularities (enhanced heat transfer, boundary layer development...) arising from turbulence while keeping a low computational cost (coarse mesh), a turbulence model is added. For solid propellant applications, the $k-\omega$ SST (shear stress transport) URANS model is adopted. It is better suited for near wall flows compared to the classical $k-\epsilon$ formulation, and recovers the good accuracy of the latter outside of the boundary layers. It is known to behave well for separating flows, adverse pressure gradients and recirculation areas compared to the other two-equations models [22].

For the sake of simplicity, we do not present the transport equations of the $k-\omega$ SST model for the turbulence related scalars k and ω, which are detailed in [22]. We only recall the laminar conservation equations for mass, species, momentum (j-th direction), total energy e_t, written here using Einstein notations, separating the Euler flow, diffusive, and source term contributions:

$$\frac{\partial}{\partial t}\begin{pmatrix}\rho\\ \rho Y_k\\ \rho u_j\\ \rho e_t\end{pmatrix}=\begin{pmatrix}-\frac{\partial \rho u_i}{\partial x_i}\\ -\frac{\partial \rho u_i Y_k}{\partial x_i}\\ -\frac{\partial \rho u_i u_j}{\partial x_i}-\frac{\partial P}{\partial x_j}\\ -\frac{\partial \rho u_i e_t}{\partial x_i}-\frac{\partial P\delta_{ij}u_i}{\partial x_j}\end{pmatrix}+\begin{pmatrix}0\\ -\frac{\partial J_{k,i}}{\partial x_i}\\ \frac{\partial \tau_{ij}}{\partial x_i}\\ -\frac{\partial}{\partial x_i}\left(-\lambda\frac{\partial T}{\partial x_i}+\sum_{k=1}^{n_e}h_k J_{k,i}\right)+\frac{\partial \tau_{ij}u_i}{\partial x_j}\end{pmatrix}+\begin{pmatrix}0\\ \omega_k\\ 0\\ 0\end{pmatrix} \tag{1}$$

The viscous tensor τ_{ij} is computed as $\tau_{ij}=2\mu\mathcal{D}_{ij}$ where the deviator tensor is defined as $\mathcal{D}=S-\frac{1}{3}tr(S)\mathbb{I}$ with $S=\frac{1}{2}\left(\vec{\nabla}\vec{u}+(\vec{\nabla}\vec{u})^t\right)$. The mixture is composed of n_e species. The term $J_{k,i}$ is the component in the i-th direction of the diffusion flux vector $\vec{J}_k$ for the k-th species is approximated by a generalised Fick's law: $\vec{J}_k=-\rho\Sigma_{j=1}^{n_e}D_{kj}\vec{\nabla}Y_j$, where the D_{kj}'s are the components of the species diffusion matrix. The volumetric production rate of the k-th species is ω_k. The enthalpy h is the sum of the chemical and sensible enthalpies: $h=\Sigma_{k=1}^{n_e}Y_k h_k$, where $h_k=\Delta h_k^0+\int_{T_{std}}^{T}c_{p,k}(a)da$, with $c_{p,k}$ the heat capacity of the k-th species, and Δh_k^0 its formation enthalpy at T_{std} the standard temperature. The thermal conductivity is λ, and the pressure if P. The Kronecker symbol is δ_{ij}. Soret and Dufour effects are neglected. The model does not account for gas phase and surface radiation. Finally, the ideal gas law relates the various state variables

in the gas phase:

$$\rho = P / \left(RT \sum_{k=1}^{n_e} \frac{Y_k}{\mathscr{M}_k} \right) \tag{2}$$

with $\mathscr{M}_k$ the molar mass of the k-th species, and R the universal gas constant.

2. Solid propellant model

This model describes the evolution of the thermal profile within the solid propellant. Due to the insulating nature of the propellant, the thickness of the thermal profile is typically on the order of 100 μm and is very small compared to other characteristic scales of the flow and motor. Consequently, as in most ignition models from the literature, we assume that heat diffusion only occurs in the direction normal to the surface, neglecting lateral heat transfer within the solid. In-depth thermal degradation of the propellant is not considered.

Following the one-dimensional heat transfer assumption, we only describe the thermal profile by the temperature field $T(x, y, z, \eta)$, with (x, y, z) the position of the surface point considered, and η the coordinate along the normal to the surface (negative towards the propellant). The propellant surface is kept at $\eta = 0$ via a change of variable [19], which introduces additional convective terms in the model equations. The solid phase at $\eta < 0$ is assumed semi-infinite, inert and homogeneous. Its temperature field T is subject to:

$$\rho_c c_c \partial_t T_c + \rho_c c_c r \partial_\eta T_c - \partial_\eta \left(\lambda_c \partial_\eta T_c \right) = 0 \tag{3}$$

with ρ_c the propellant density, c_c its heat capacity, λ_c the thermal conductivity, and r the absolute surface regression speed, deduced from Eq. (9) in the next section. Far below the surface, the solid is at its resting temperature:

$$T_c(-\infty) = T_i \tag{4}$$

3. Surface connection conditions

The fluid and solid models are connected at the surface of the solid propellant. In reality, this interface may be a so-called "foam" zone, a thin layer where liquid and gas phases coexist. However, its properties and behaviour are not well established, hence we simplify its modelling by representing this zone as an infinitely thin layer where all the pyrolysis and gasification processes occur. The surface variables are identified by the subscript s.

Surface balance along the normal vector We use the subscript s to identify the values that are taken at the surface for the solid propellant model, i.e. at $\eta = 0$. The connection of the gas and solid phases at the interface is given by the following conditions, expressing the continuity of the mass flow rate and temperature, as well as the enthalpy and species fluxes balance around the interface:

$$\begin{cases} \rho_c r = m(0^+) & (5) \\ T(0^-) = T(0^+) = T_s & (6) \\ \left(mh - \lambda_c \partial_\eta T \right)_{0^-} = \vec{n}. \left(mh\vec{n} - \lambda \vec{\nabla} T + \Sigma_1^{n_e} h_k \vec{J_k} \right)_{0^+} & (7) \\ \left(mY_{inj,k} \right)_{0^-} = \vec{n}. \left(mY_k \vec{n} + \vec{J_k} \right)_{0^+} \quad \forall\, k \in [\![1, n_e]\!] & (8) \end{cases}$$

with $\vec{n}$ the normal unit vector oriented towards the $\eta > 0$ (inside of the CFD domain), m the mass flow rate ($\rho_c r$ in the solid, ρu in the gas) and Y_{inj} the product mass fractions generated by the decomposition and gasification processes, which can be constants or functions of the surface temperature as in [23].

The surface mass flow rate is given by the pyrolysis law:

$$m(0) = m_s = \rho_c r = f(T_s, P) \tag{9}$$

In the simulations presented further in the present paper, we only consider finely resolved meshes such that the turbulent viscosity μ_t is correctly driven to 0 at the surface. Indeed, the mesh spacing required in practice to properly resolve the propellant flame is such that the near-surface flow field is very well resolved (typically $y^+ \approx 0.1$). This enables us to only consider the laminar expression of the fluxes at the surface.

Boundary conditions for the fluid model The fluid model is multi-dimensional, hence additional boundary conditions are required, in particular for the momentum equation, as well as for the turbulence-specific conservation equations. We use the subscript w to denote the parietal (wall) values used in the fluid model, which in the case of this detailed modelling, will be identical to the values at the propellant surface model (subscript s). We assume that gaseous species that leave the surface are injected in the direction perpendicular to the propellant boundary face. We impose a no-slip condition at the surface, i.e. the fluid flow velocity must tend to the surface injection velocity vector $\vec{u}_w$:

$$\vec{u}_w = \frac{m_s}{\rho_w}\,\vec{n} \tag{10}$$

The parietal values of the turbulent variables k and ω are user-specified constants.

B. One-dimensional propellant flame modelling

The gaseous products generated by the surface pyrolysis react and form a flame which is typically a few hundred micrometers thick. Its accurate capture within a simulation therefore requires a very refined mesh near the propellant surface (typically 1 μm thick cells locally). Moreover, if detailed kinetics are used for this flame, the computational expense of evaluating the corresponding reaction rates within the chamber flow field solver can be very large. Thus, capturing the propellant flame and combustion chamber flow field within a fluid model induces strong computational requirements, typically preventing the feasibility of a complete chamber ignition simulation in 3D.

As the propellant flame is very thin compared to the chamber characteristic length scale ($\approx$ 1 m), it could be computationally interesting to discard the gaseous reactions from the fluid model, and insert an additional surface model that solves the propellant flame independently. For homogeneous propellants, the flame can typically be considered one-dimensional, in a similar fashion as done for the heat diffusion within the solid propellant. Heterogeneous propellants such as AP-HTPB can also be represented accurately by 1D models over a wide range of pressures [24]. Finally, the Mach number in the flame zone is typically very small, hence the fully compressible framework of the initial fluid model from Section II.A.1 can be simplified by considering a low-Mach number flow, avoiding computational constraints associated with pressure waves. A simplified flame model can then be formulated. The space coordinate along the one-dimensional flame is η as for the solid phase, since the same change of variable is performed to track the interface. The flame at $\eta > 0$ is modelled a low-Mach reactive flow, subject to the following partial differential equations:

$$\begin{cases} \partial_t \rho + \partial_\eta(\rho(u+r)) = 0 & (11)\\ \partial_t \rho Y_k + \partial_\eta(\rho(u+r)Y_k) = -\partial_\eta J_k + \omega_k \qquad \forall k \in [\![1, n_e]\!] & (12)\\ \partial_t \rho h + \partial_\eta(\rho(u+r)h) = -\partial_t P - \partial_\eta(-\lambda\partial_\eta T + \Sigma_1^{n_e} h_k J_k) & (13) \end{cases}$$

In previous work [19, 20], we have conducted extensive analysis of this flame model, demonstrating its well-posedness, its specific mathematical properties, which requires specific numerical methods (see Section III.A.2) and its relevance for solid propellant applications.

This flame model is inserted as an additional modelling layer between the fluid and surface models. The surface connection conditions must now be applied between the solid model from Section II.A.2 and the 1D flame model. The field variables of the 1D flame model replace the ones of the chamber fluid model in the right-hand sides of Eqs. (5)–(8).

New connection conditions must be provided to link the 1D flame and chamber fluid models. In practice, to ensure the propellant flame is entirely captured within the 1D flame model, the 1D domain extends much further than the typical flame height, so that chemical equilibrium is reached, allowing for the flame-related kinetics to be discarded from the fluid model. This introduces specific difficulties regarding the temporal coherence and conservativity of the coupling between the flame and fluid models, which we avoid by enforcing the quasi-steadiness of the 1D flame, setting all time derivatives in Eqs. (11)–(13) to 0. This matter is discussed in detail in Appendix V. The 1D chamber fluid prescribes the value of the parietal pressure P_w as the value of the thermodynamic pressure P in the whole 1D gas domain. In return, the 1D flame model transmits flow rates of mass, species and energy. From the point of view of the fluid model, the propellant surface is still considered as an adherence surface, however the parietal values of the field variables are set to the values of the same fields at the exit of the 1D gas phase (subscript f). Chemical equilibrium being reached within the 1D gas phase, the exit boundary conditions for the 1D flame are simple Neumann conditions:

$$\partial_\eta T(+\infty) = 0, \qquad \partial_\eta Y_k(+\infty) = 0 \qquad \forall k \in [\![1, n_e]\!] \tag{14}$$

Therefore, no diffusive fluxes leave the 1D flame model, only convective fluxes. To ensure physical coherence of the coupling, surface species diffusion fluxes are set to 0 for the fluid model as well. Due to the previous modelling choices,

the conjugate heat transfer between the fluid model and solid models cannot be captured by the 1D flame model. It must be handled by reintroducing a direct connection between the fluid and solid models. This is done by inserting the wall heat flux from the fluid model into the surface coupling condition (7). This wall heat flux is computed as:

$$\Phi_w = \lambda \vec{\nabla} T . \vec{n} = \left(\lambda \partial_\eta T\right)_w \tag{15}$$

We stress that the temperature field used in this last equation is the one of the fluid model, not the 1D flame. The heat flux is evaluated at the surface, i.e. for $\eta = 0$. It is then added to the surface enthalpy balance (7), forming the following modified equation:

$$\left(mh - \lambda_c \partial_\eta T\right)_{0^-} = \left(mh - \lambda \partial_\eta T + \Sigma_1^{n_e} h_k J_k\right)_{0^+} - \Phi_w \tag{16}$$

Note that surface friction power also increases the wall heat flux, however its contribution is usually 3 to 5 orders of magnitude lower than that of the conductive heat flux, hence we do not include it in Eq. (15).

Finally, the surface viscous fluxes for the fluid model are expressed by assuming adherence at the wall, and the injection velocity is defined as in Eq. (10).

In practice, part of the intent of having such a model is to reduce the CFD mesh refinement for the fluid model near the wall. This is possible thanks to the flame not appearing within the fluid domain any more. Further gains could be obtained by reducing the mesh refinement below the one classically required for an accurate computation of the conjugate heat-transfer ($y^+ \approx 1$). This would however necessitate the use of wall laws to maintain an accurate wall heat flux. This introduces additional complexity to the model, therefore we do not consider that issue further in this work.

III. Coupled framework for SRM ignition simulations

To simulate the previous models, we choose to avoid a monolithic approach where all the models are solved within one single solver. We rather capitalize on the codes already developed at ONERA, only requiring the specific surface coupling conditions to be implemented. In this section, we present the various solvers, before presenting the coupling procedure.

A. Available solvers

The previous models have been implemented in two separate solvers. The fluid model is implemented in the CFD code CHARME from ONERA, and the combination of the propellant, surface and 1D flame models are implemented in the Vulc1D code. Both solvers are presented in the following.

1. Fluid solver

The fluid model for the combustion chamber flow field is implemented in the CFD solver CHARME from ONERA, which is described in [21]. CHARME uses the cell-centered finite volume technique on general unstructured meshes to semi-discretise in space the set of conservation equations (1). A second-order MUSCL scheme with multislope reconstruction [25] is used to compute the values of the field variables on each side of every mesh face, and various limiters can be applied to ensure the total-variation-diminishing (TVD) character of the scheme. The associated Riemann problems are solved with the approximate Riemann solver HLLC to compute the Euler fluxes at each face, and the diffusive fluxes are evaluated using a second-order centered scheme. A wide variety of boundary conditions are available, e.g. symmetry, heat transfer, non-reflection, porous walls.

For the temporal discretisation, several linearised implicit Runge-Kutta methods can be applied, of order one or two. The implicit system obtained at each time step is solved with the help of the Generalized Minimal Residual method (GMRES). Explicit Runge-Kutta methods from order 1 to 4 are also available, however they will not be used for the present work, due to the excessive stability restrictions when dealing with fine meshes. Parallelisation is enabled via the use of MPI directives.

CHARME is fully integrated within the multiphysics simulation semi-industrial toolchain CEDRE [21], allowing for it to be coupled with other codes, such as radiation or polydisperse spray solvers. CEDRE is routinely used at ONERA and collaborators for a wide variety of studies, e.g. subsonic to hypersonic aerodynamics, combustion chambers, multiphase flows.

2. Solid propellant solver

The complete one-dimensional model propellant combustion model (solid, surface, and flame) is implemented and solved in the Vulc1D code. We recall the main aspects of the numerical strategy for the implementation of this model as a standalone tool, which is explained in greater detail in [20]. The previous conservation equations are semi-discretised in space using a finite-volume approach on a staggered grid, with the temperature and mass fractions stored at the cell centers, and the mass flow rate located at the cell faces. Diffusive fluxes are approximated by a second-order centered scheme. Convective fluxes are discretised either using a first-order upwind scheme, or a second-order centered scheme when the local cell Péclet number is low enough, i.e. if the mesh is locally well refined.

The set of semi-discretised equations form a system of differential-algebraic equations (DAEs) of index 1, i.e. some variables (the surface variables T_s, $Y_{s,k}$ and the gas phase mass flow rate discrete values) are not governed by ODEs that give their time derivatives directly, but are constrained by algebraic equations. They must continuously adapt to the evolution of the other variables to ensure the surface balance equations (5)–(8) and the gas phase continuity equation (11) are satisfied. This specific nature has been explicitly identified in our aforementioned work [20] and requires carefully chosen time integrators so that the solution method is consistent, stable, precise and efficient. We have chosen to use high-order singly diagonal implicit Runge-Kutta methods with an explicit first stage (ESDIRK [26]) and we have shown their high efficiency, stability and precision. Time step adaptation is possible thanks to the inclusion of an embedded scheme of lower-order that allows for the construction of an estimate of the local truncation error. The overall implicit system is solved with a damped Newton method. The corresponding Jacobian is block-tridiagonal and each Newton step is solved using a Thomas algorithm.

B. Coupling methodology

The previous solvers can be coupled to compute the ignition of a combustion chamber. The underlying idea is the same as for the various large-scale ignition simulations presented since the 1990s [5, 14]. The combustion chamber is meshed in 2D or 3D and its internal flow field is simulated with the CFD solver. At each boundary face corresponding to the propellant surface, an instance of the one-dimensional propellant solver is used to compute the evolution of the thermal profile within the propellant and the combustion of the latter. At each time step of the coupled computation, the coupling variables and fluxes are exchanged between both solvers.

Following the various modelling levels presented in the Section II, two approaches are designed. The first approach, referred to as *detailed coupling*, uses the most detailed modelling, with the propellant flame being handled in the fluid model. Vulc1D is used to compute the evolution of the thermal profile inside the propellant and of the surface variables, but its 1D gas phase is discarded. The 1D model provides the surface variables (temperature, mass flow rate, composition) and surface fluxes which are used as boundary conditions for the fluid model.

In the second approach, referred to as *1D flame coupled approach*, the flame is modelled using the model from Section II.B. The fluid model transmits the value of the parietal pressure and heat flux. However, for the fluid model boundary condition, the parietal variables are set to their value at the end of the 1D gas domain instead of at the propellant surface. This approach is conceptually similar to the other ignition models from the literature already mentioned in the introduction. These use a quasi-steady burn rate law to avoid a more complex modelling of the propellant flame, however the modelling choice is essentially the same: the flame is represented within the boundary model, not within the CFD domain. Thus the CFD domain does not need to be meshed very finely near the surface, and the CFD solver can work only with inert combustion products, sparing the computational expense of evaluating chemical source terms over the whole domain. Another advantage of our approach is the ability of the 1D flame model to use a more refined representation of the propellant flame if required, for instance by including detailed transport.

C. Coupling in time

To produce a time-accurate simulation of the overall combustion chamber ignition, the previous fluxes exchange must be performed periodically. This is done at each so-called coupling time step Δt, as depicted in Fig. 1. At each time step, the CFD solver CHARME transmits the parietal pressure P_w, the heat flux Φ_w (and potentially a radiative heat flux) to the propellant solver Vulc1D. This solver then proceeds forward in time for one coupling time step, and gives back to CHARME a flow rate of mass, species, and enthalpy, which are injected through the previously described boundary conditions in CHARME. CHARME can then move forward one step, and the whole process starts over again for the next coupling time step.

To improve the stability and precision of the computation, while also easing the simulation set-up, the coupling time step is dynamically selected such that the relative solution variation is limited to a given value (typically 2%) in all CFD

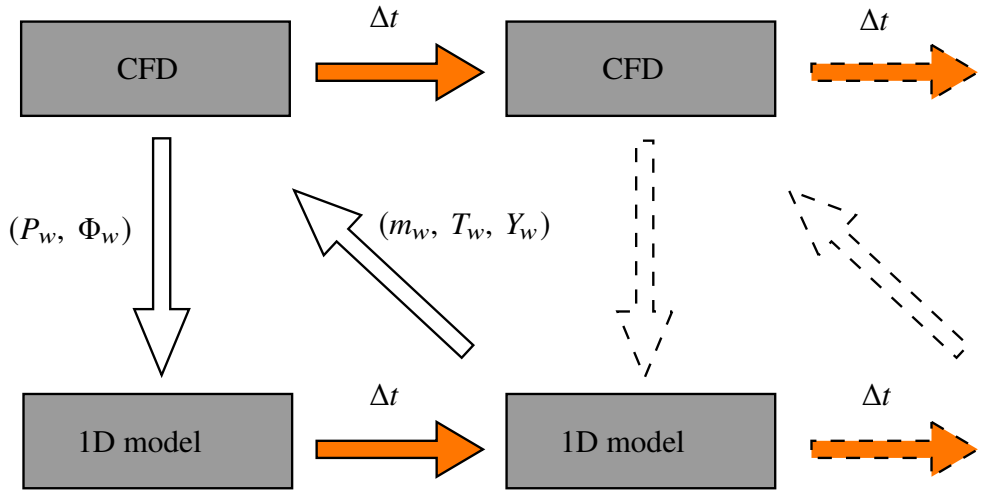

Fig. 1 Coupling algorithm between Vulc1D and CHARME

cells. Thus the near-surface cells typically dictate the overall time step.

The coupling algorithm is first-order in time, and corresponds to a single Gauss-Seidel iteration of a waveform relaxation approach. Therefore, we only use a first-order accurate time scheme (backward Euler) in CHARME and Vulc1D for the coupled simulations, and each solver only performs one time step per coupling step. Extensions of the present coupling to higher-order is the subject of ongoing research, with the added ability for each solver to perform as many substeps as required to satisfy a given error tolerance [27, 28].

D. One-dimensional verification

We now verify the implementation of the previous models in a one-dimensional case of laser-induced ignition, i.e. with an additional constant heat flux imposed at the propellant surface.

1. Model parameters

We consider a simple model of an AP-HTPB-Al propellant, which is a slight variation of the one used in [19, 20]. The main characteristics of the simplified model are summarised hereafter.

Solid phase The solid phase is composed of the solid species P and has the following properties: $\rho_c = 1800$ kg.m^3, $\Delta h_f^o(c) = 0$ J/kg at $T = 0$ K, $c_c = 1150$ J/kg/K, $\lambda_c = 0.55$ W/m/K. The initial temperature is $T_i = 300$ K.

Surface The pyrolysis mass flow rate is computed as: $m_s = A_p T_s^\beta \exp(-T_{ap}/T_s)$, with $A_p = 1 \times 10^9$ kg/s/m^2, $\beta = 0.3$ and $T_{ap} = 1.5 \times 10^4$ K. The pyrolysis process converts the solid phase into the gaseous species G_1.

Gas phase Two global species are considered: the reactant G_1 and product G_2, which have the same properties except standard enthalpies. Their molar mass is $\mathscr{M} = 27$ g/mol, and their heat capacities are $c_p = 2800$ J/kg/K. The standard enthalpies at $T = 0$ K are $\Delta h_f^o(G_1) = 0$ J/kg et $\Delta h_f^o(G_2) = -8.9 \times 10^6$ J/kg. The unique global reaction is $G_1 \longrightarrow G_2$ and irreversible. The reaction rate is computed as: $\omega = A[G_1]^n T \exp(-T_a/T)$, with $A = 2750$ s^{-1}, $T_a = 1500$ K, $n = 0.6$ and $[G_1]$ the concentration of G_1. The diffusion coefficients are equal for both species and taken as a linear function of T such that the Schmidt and Prandtl numbers remain constant (1 and 0.5 respectively). The thermal conductivity is $\lambda = 0.45$ W/m/K.

2. Simulation of laser-induced ignition

The solid propellant solver has already been verified in [20] for the laser-induced ignition of a propellant sample. Thanks to its time adaptation capability and high-order temporal schemes, as well as the use of a highly-refined 1D

mesh, the obtained solution is very precise and can be used as a reference. The previously presented coupled approaches can then be tested with a similar physical configuration to verify their ability to reproduce the one-dimensional ignition, using CHARME to solve the gas phase dynamics.

Both the standalone Vulc1D code and the coupled framework are parametrised with the previous model parameters. The gas phase is at 5 bars, and the initial temperature field is uniform at $T = 300$ K, both in the solid and gas phases. The gas is initially composed only of combustion products G_2 that act as the initial pressurisation inert gas. For the coupled approaches, the CFD mesh has cells with a geometrical progression in thickness. For the 1D coupled flame approach, the size of the first cell above the surface is 10μm, which is sufficient to accurately capture the heat loss via diffusion through the gas phase during the initial heating of the surface. For the detailed coupled approach, the proper resolution of the propellant flame in the CFD domain requires a finer mesh, thus the first cell is reduced to 1μm.

At $t = 0$ s, a 1 MW.m^{-2} laser heat flux is applied at the propellant surface via an additional heat flux, inserted in the surface balance equation (7) as previously done for Φ_w. The surface temperature rises, some energy being lost via diffusive heat transfer to the gas phase. At one point, the pyrolysis mass flow rate becomes important and a sufficient amount of gaseous reactants is expelled from the surface, forming a flame that attaches to the surface, causing a rapid increase in surface temperature. Finally, the system converges to steady state.

The obtained surface temperature evolutions are shown in Fig. 2. The reference result is the orange curve, which is obtained with Vulc1D only, solving both the unsteady solid and unsteady gas phase with a fifth-order adaptive time scheme. The dashed curves are obtained with the two coupled approaches, which are first-order in time. The green dashed curve is obtained with the detailed coupled approach. The ignition time is 0.9% larger than the reference result, which may be attributed to the coarser gas mesh used in the coupled approach. The red dashed curve is obtained with the 1D flame coupled approach, with a quasi-steady flame. The heat loss at the surface via diffusion to the CFD gas phase is correctly captured, and ignition occurs 0.8% faster than in the reference simulation. This may be attributed to the faster appearance of the propellant flame, following the quasi-steady assumption.

We have also added the blue curve of T_s obtained with Vulc1D only and a quasi-steady gas phase, using a fifth-order adaptive time scheme. We observe that, before ignition, the temperature rises more quickly. This is due to the lack of diffusive heat loss to the gas phase, as the quasi-steady flame model results in a uniform gas temperature field at $T = T_s$ before ignition. Therefore the point of ignition is reached more quickly, in this case 12 % faster than in the reference simulation.

Consequently, the quasi-steady assumption used for the 1D flame in the coupled approach does not modify much the overall ignition behaviour. Indeed the heat loss by diffusion to the gas phase can still be captured by the direct connection between the fluid and propellant models via the heat flux Φ_w in Eq. 16. Note however that the flame appearance is faster in quasi-steady mode, so there might be a more visible difference in a configuration where the development time of the unsteady flame is not small compared to the characteristic time of ignition.

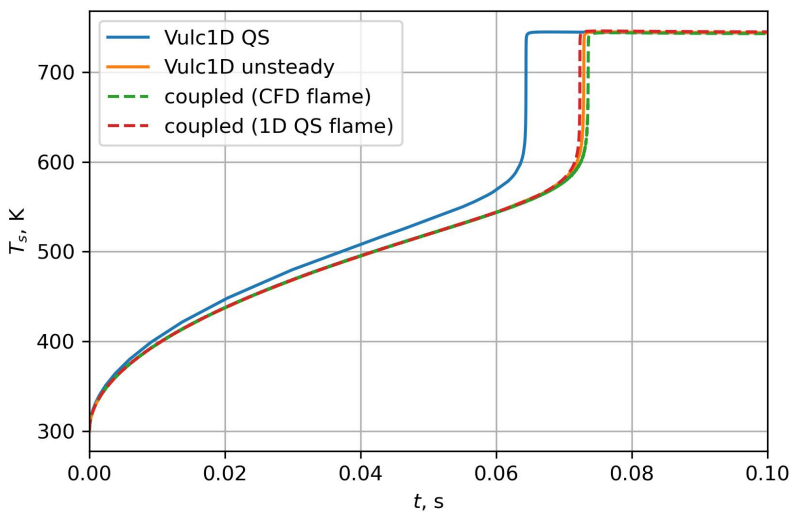

Fig. 2 Comparison of the surface temperature evolutions for the laser-induced ignition

IV. Two-dimensional test case with igniter flow

We now present a two-dimensional configuration, which we have designed such as it is representative of a solid rocket combustion chamber. The introduction of an igniter jet leads to a complex flow field which features instabilities and recirculation areas, making it a very relevant case for the study of ignition. Both coupled approaches are used, and their results are compared. This section provides several contributions. To our knowledge, this is the first reported use of a detailed approach for the simulation of ignition in a small chamber. This is also the first comparison between this detailed approach and the 1D flame coupled approach, the results of which are particularly important to validate the use of the latter for large-scale ignition simulation.

A. Definition of the test case

We consider a simplified configuration, representative of the impingement region of the igniter flow in a SRM combustion chamber. We consider a 2D axisymmetric rectangular domain, the lower boundary of which corresponds to a solid propellant surface. The left boundary is a wall boundary, with an opening in the middle where the igniter flow is injected at $T = 2300$ K with a mass flow rate of 110 kg.m^2.s^{-1} and an angle of 45 degrees. The right boundary is a subsonic outflow condition, with a prescribed pressure of 5 MPa. The upper boundary is a symmetry boundary.

The mesh is unstructured and composed of quadrangles, with the exception of the 200 μm thick zone above the propellant, which is meshed in a cartesian manner. The first layer of cells above the propellant has a thickness $\delta = 1$ μm, and the cell thickness progressively increases further away from the propellant. This allows for a fine spatial resolution of the near-surface hydrodynamics, in particular the conjugate heat transfer, and also of the gaseous flame (for the detailed approach). The equivalent diameter of the mesh cells is plotted in Fig. 3. The mesh is highly refined in the vicinity of the igniter flow and near the surface, so as to correctly resolve all the flow scales in this area. A posteriori analysis show that this near-surface refinement yields $y^+ \leq 0.1$, hence the boundary layer is correctly resolved in this URANS context. The total number of cells in the CFD domain is 4.7×10^5. Each 1D propellant model has 60 cells for the solid phase, and 200 cells for the 1D flame (if activated).

For the simulations with the 1D flame approach, issues with numerical stability of the current coupling have constrained us to used a slightly coarser mesh near the surface. Indeed, the current implementation of the 1D flame coupled approach does not allow Vulc1D to handle the wall heat flux Φ_w implicitly in Eq. (16). This flux is therefore explicit and, when its value is too high, temperature oscillations start to appear in Vulc1D and CHARME near the surface. This issue has been strongly mitigated by setting the first cell height to 4 μm, which is still fine enough to resolve the near-surface flow dynamics. The unstructured part of the mesh remains unchanged.

In both meshes, the surface is discretised in 5062 boundary faces, each associated with an instance of the one-dimensional model. The first 5000 thousands boundary cells from $x = 0$ m to $x = 0.1$ m have a length of 20 μm in both cases. From $x = 0.1$ m to $x = 0.17$ m, the mesh is gradually coarsened, such that only 62 boundary faces are added.

The initial state is uniform at 5 MPa, zero velocity, and $T = 293$ K in the fluid. The solid propellant is also initialised at $T = 293$ K. We use the same physico-chemical modelling presented in Section III.D.1. Initially, only combustion products G_2 are present. The igniter flow also injects the same combustion products. The reactant species G_1 only appears near the surface in the simulation with the detailed coupling.

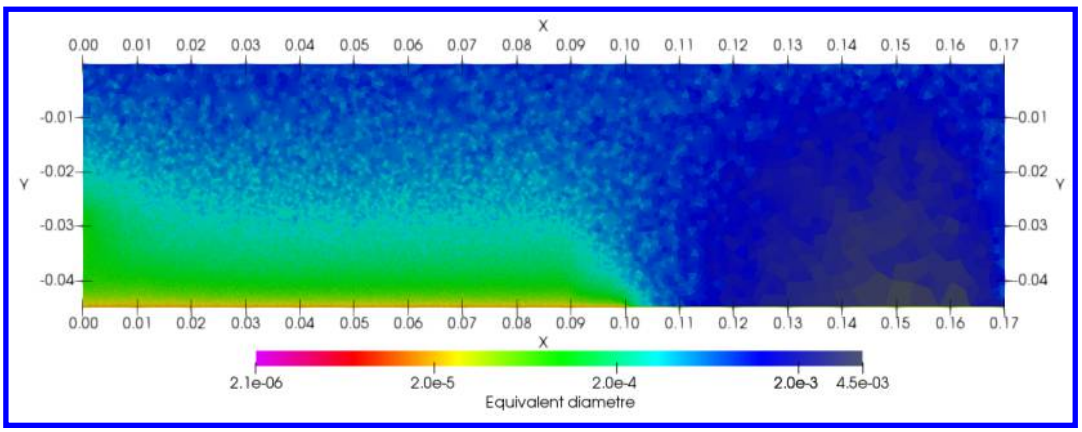

Fig. 3 Equivalent cell diameter in the CFD mesh

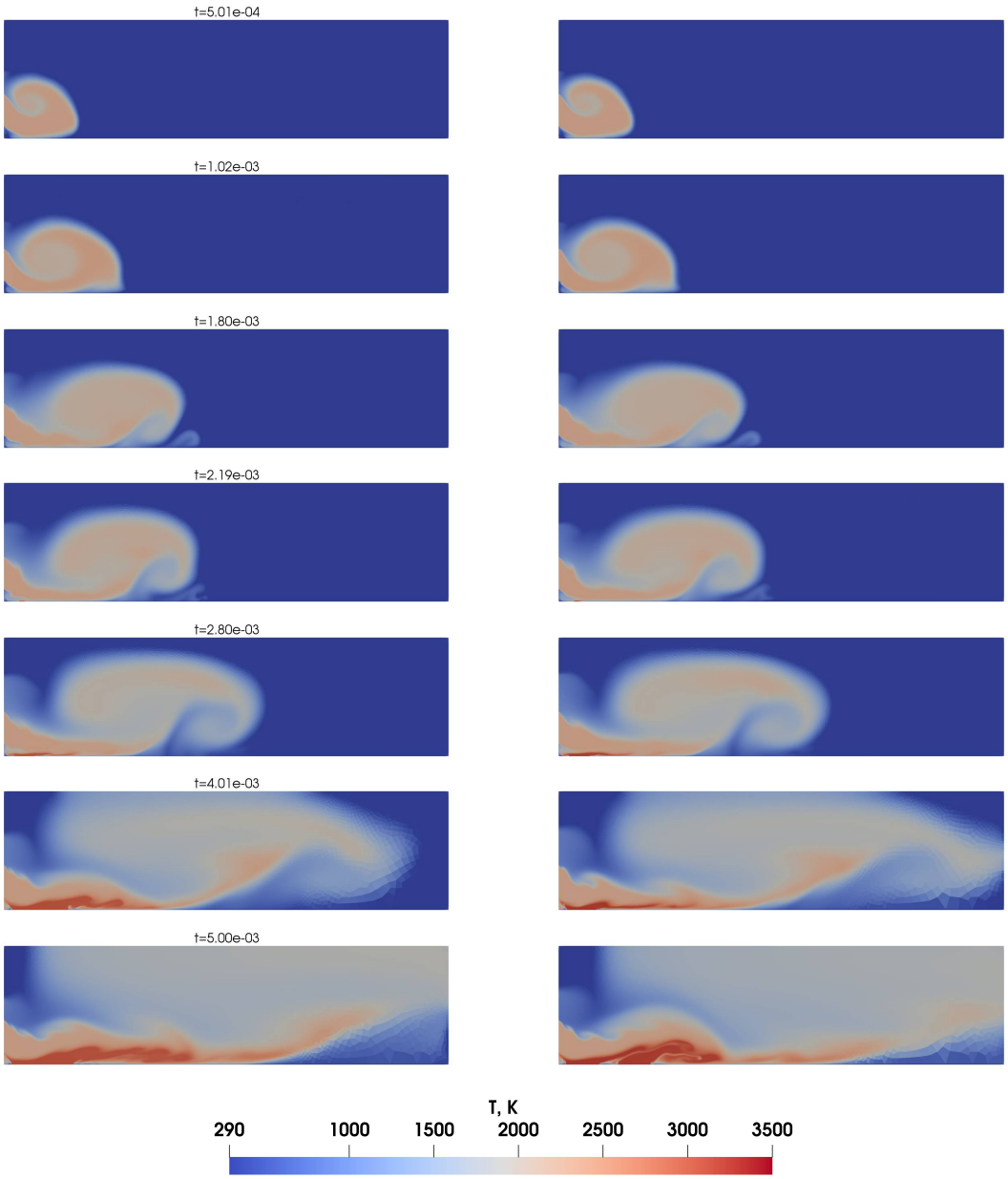

Fig. 4 Evolution of the temperature field (left: detailed coupling, right: 1D flame coupling). Time is given in seconds.

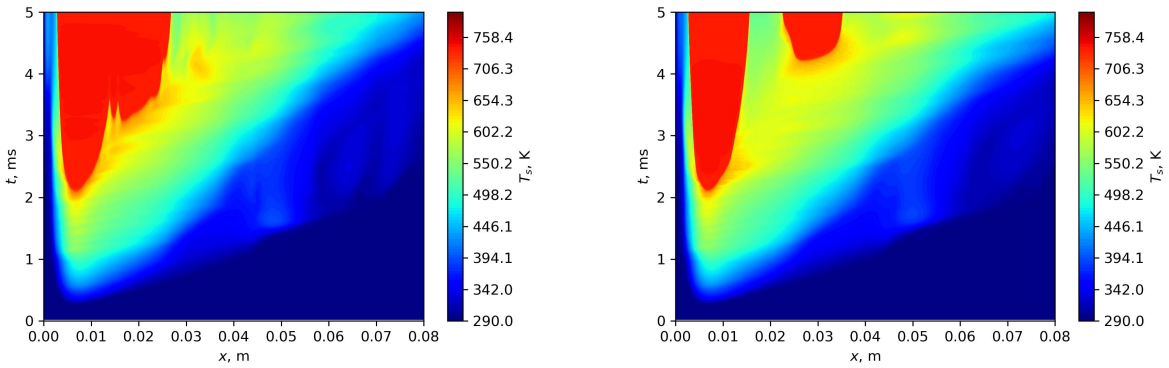

(a) Detailed coupled approach $\delta = 1$ μm **(b) 1D flame coupled approach $\delta = 4$ μm**

Fig. 5 Evolution of the propellant surface temperature

B. Comparison of both approaches

The computation is conducted for a physical time of 5 ms. Various snapshots of the temperature flow field are shown in Fig. 4. To better visualize the heating of the propellant surface and the propagation of ignition, Fig. 5 shows a space-time diagram of the evolution of the surface temperature. This allows for a clear representation of the ignited zones and of the temporal evolution of the grain preheating.

First, we can observe that both results are in excellent agreement for the first 3 ms. In particular, the initial heating induced by the igniter jet results in the same surface temperature increase. Ignition occurs at the same time ($t \approx 2.1$ ms) in both cases and at the same location. The subsequent initial flame spread is also identical. Furthermore, the chamber flow field is very similar between the two solution methods. Ignition occurs in both cases at the same time ($t \approx 2.1$ ms) and at the same location ($x \approx 0.007$ m). This indicates that the 1D flame approach enables an accurate capture of the grain preheating, and that the necessary transition of its wall heat flux formulation during ignition, as discussed in Appendix V, is correct.

Some time after ignition, the flow fields start to diverge slightly. This can be explained by several phenomena.

The main reason seems to be that, with the 1D coupled flame setup, the first ignited zone temporarily has a slightly higher surface temperature and mass flow rate near $t \approx 2.5$ ms. This may be attributed to a poorer spatial resolution of the flame in the CFD mesh compared to the 1D gas domain, the first cell size of which is 100 times smaller. It can lead to lower flame heat-feedback, hence a slightly lower surface temperature and pyrolysis flow rate.

Second, the flow field features an unstable igniter jet. Any small variation of the flow near the surface can cause the unstable jet to behave differently, as is clearly seen in the lower snapshots from Fig. 4. An additional effect comes from the jet deflection due to mass flow rate injected at the propellant surface. This creates a recirculation zone ahead of the ignition front, which also increases the overall sensitivity of the surface ignition. This is seen for example in Fig. 2 at $t \approx 4.1$ ms and $x \approx 0.033$ m. With the detailed approach the first ignition zone to the left is larger and causes the igniter jet flow to be deflected slightly too much, such that the surface, which had already been heated up to $T_s \approx 650$ K locally, is momentarily cooled down. On the contrary, the 1D flame coupled approach has a first ignition zone which spreads slightly less, hence this cooling does not occur and a second ignited zone appears.

Third, the surface friction is different between both approaches, as the parietal flow speed is not the same in both simulations. Indeed, both approaches inject in the CFD domain the same mass flow rate, but not the same temperature, hence parietal densities are not the same: their ratios is obtained from the ideal gas law (2) as the ratio T_s/T_f. This is due to the fact the 1D flame model already accounts for thermal expansion, whereas this occurs within the flame in the CFD domain for the coupled approach. Consequently, the injection speed is roughly 4 times faster with the 1D coupled flame approach, and the friction forces differ.

Finally, numerical experiments have shown that the solution flow field was slightly impacted by the time step used for the simulations, in particular due to the use of a first-order time scheme, and a poorer stability of the 1D coupled approach compared to the detailed one, due to the previously mentioned technical difficulties with the implicit handling of the wall heat flux for Vulc1D.

C. Effect of a lower near–surface mesh refinement

Another simulation has been conducted on a third mesh, where the 200 μm zone above the propellant is meshed with 20 μm thick cells, while maintaining the same 20 μm longitudinal refinement. The rest of the unstructured mesh is unchanged. Fig 6 shows the temporal evolution of the leftmost and rightmost ignited abscissa along the propellant surface. Again, we clearly the excellent agreement between the 1D flame approach on a fine mesh (δ = 4 μm) and the detailed coupled approach (δ = 1 μm). With the third mesh (δ = 20 μm), the first ignition occurs slightly sooner at the same point, and the flame propagation along the surface is faster, which has a great impact on the dynamics of the chamber flow field. The simulation with δ = 20 μm however does not capture the initial conjugate heat transfer. The wall heat flux is slightly higher across the whole surface at all times. This causes the first ignition to appear sooner, and the subsequent flame spread is facilitated by the larger preheating.

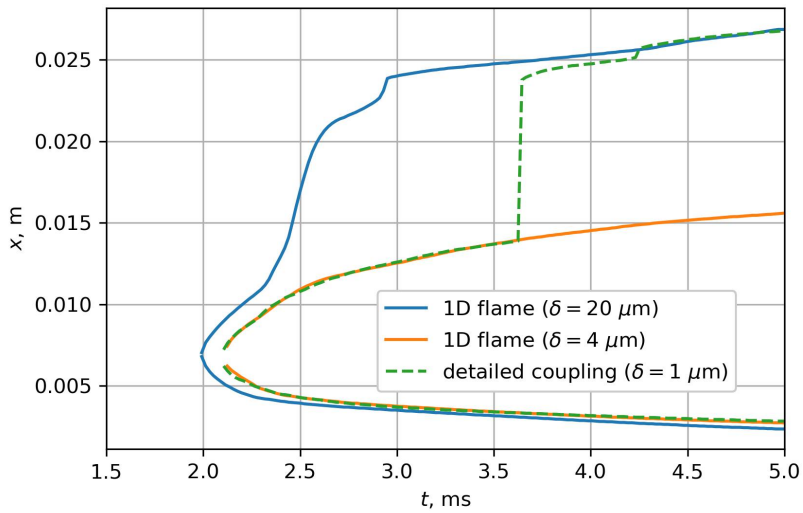

Fig. 6 Temporal evolution of the outermost ignited positions for 3 combinations of coupled approach and mesh refinement.

Note that δ = 20 μm does not allow for an accurate resolution of the conjugate heat-transfer any more. As discussed in Section II.B, this could be mitigated by using wall laws. This would however require a finely-tuned wall law, which is out of the scope of this paper.

Overall, this test case proves to be very discriminant, as slight solution discrepancies are quickly amplified. Additionally, the proper resolution of the flow field and heat transfer requires a well refined mesh.

V. Conclusion

A new strategy for the simulation of solid rocket motors at large-scale has been presented. Compared to the strategies previously described in the literature, the main improvement is the ability to solve the propellant flame numerically, without resorting to very simplified flame models. In particular, the modelling level used in the one-dimensional flame model can be changed easily, allowing for both simple or detailed kinetics to be handled. To better assess the impact of the one-dimensionality of the flame as well as its quasi-steadiness, required to ensure overall energy conservation and temporal coherence, a reference coupling strategy has also been developed, where all gas phase phenomena are solved within the CFD solver. This induces larger computational requirements, in particular for the mesh refinement, but enables a detailed simulation of the surface ignition and flame-flow interaction to be obtained. To our knowledge, using such a detailed modelling for ignition at large scale had not been previously presented in the literature.

Comparison for laser-induced ignition in 1D have shown excellent agreement between both approaches and the standalone 1D model from [20], indicating that the surface coupling is correctly implemented. This test also allows to verify that the quasi-steady assumption for the 1D flame is reasonable and does not accelerate ignition too much, however that effect may depend on the particular physico-chemical model used for the flame.

A 2D test case has been designed to feature the various phenomena encountered in SRMs: igniter jet impingement, complex hydrodynamics, flame spread. On fine meshes, both the detailed and 1D flame flame couplings produce the same flow field, first ignition point and time, and initial flame spread. Due to the high sensitivity of the chamber flow field, the solutions finally diverge from one another. To our knowledge, this is the first use a detailed approach (flame captured within the fluid solver) for the simulation of the ignition of a small chamber. This is also the first comparison between such a detailed approach and the 1D flame coupled approach. The test case has proven to be highly sensitive, in particular due to the jet instability and the 2D axisymmetric setting which allows for sustained recirculation zones to be created, isolating part of the unignited propellant surface from the igniter jet. This renders a direct comparison of the various simulations difficult beyond a certain time, as any slight difference rapidly has a noticeable impact on the overall flow field. Also, a highly refined mesh is required for an accurate capture of the conjugate heat transfer. Overall, this configuration gives a strong demonstration that the 1D flame model behaves correctly, and that it is a sensible modelling approach for large-scale ignition transient.

Further studies with various lateral and vertical near-surface mesh refinements are being conducted to assess the effect of the spatial resolution on the flame spread. The impact of the various wall heat flux transitions discussed in the Appendix will also be investigated. Radiation models available in CEDRE can easily be added to the overall modelling to account for gas and surface radiation. This will allow for radiative grain preheating to occur, which may soften the differences observed in the 2D test case, as radiation has often been reported to be an important contribution for the propagation of ignition [17].

In the present work, no wall laws have been used to improve the accuracy of the conjugate heat transfer. Future work will investigate the use of these, and the detailed coupling could be used to generate new wall laws better suited for a given configuration.

Some aspects remain difficult to model with the 1D flame approach. For instance, at the aft-end of a SRM, turbulence may impact the flame structure [29] and thus the burning rate of the propellant. Our current 1D flame model does not include any turbulence related effects, therefore is unable to reproduce such effects. The inclusion of turbulence related conservation equations in the 1D flame model could improve this aspect by providing an unsteady numerical wall law.

Finally, the presented coupling strategy is only first-order accurate in time. Both the CFD and propellant codes are able to achieve higher-order separately, hence future work will focus on enhancing the coupling process to increase the overall temporal order of the computation, as well as to enable substepping for each solver. This may greatly improve the efficiency and accuracy of the coupling and is currently work in progress [27, 28].

We believe that the present work is an important first step towards efficient and accurate simulations of the propellant heating and ignition for large-scale solid rocket motors.

Appendix

Modelling issues

To ensure the flame is entirely captured, the 1D gas mesh from the solid propellant model is extended far enough so that equilibrium is reached at its exit. Typically its length is $L = 1$ mm. Thus, all reactants are consumed and only non-reactive gases are injected into the CFD domain, sparing the computational expense of computing kinetics-related source terms in the CFD solver. This approach is exactly coherent with the other ignition models from the literature [16, 30] where the flame, be it modelled by an analytical formula, or hidden within a semi-empirical burn rate formula, is entirely contained within the solid propellant model.

However, the large extension of the 1D gas flame mesh means that there is a strong overlap between the 1D gas domain and the CFD domain. Several conceptual issues arise from this overlap. Figure 7 gives a visual picture of the spatial overlap, as well as the locations where the exchanged fluxes are applied. The cell centers of the 1D solid and gas meshes are represented by the red squares. The cell faces of the CFD mesh are represented by the thin vertical black dashed lines, and the cell centers are represented by the blue crosses. The temperature at the center of the first CFD cell is T_1.

A. Conservativity, time lag and flame quasi-steadiness

The first problem occurs if we use a fully unsteady 1D gas phase in the boundary model. In that case, a change in the parietal heat flux Φ_w or pressure P_w provided by the CFD solver has an instantaneous effect on the interface in the 1D model and on the 1D gas phase, because the 1D gas thermodynamic pressure field is uniform and equal to the

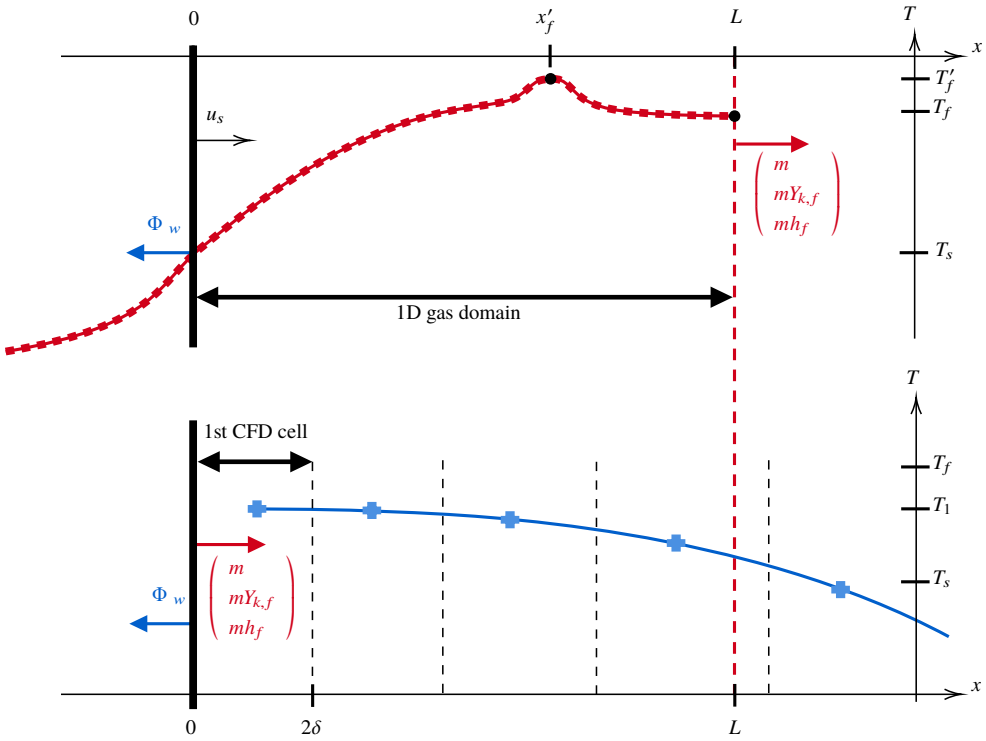

Fig. 7 Illustration of the spatial coupling between the 1D code (upper part) and the CFD code (lower part), showing the overlap of the 1D flame and the CFD domain

parietal pressure, and the wall heat flux is directly applied on the propellant interface in the 1D model (blue arrow in Fig. 7). However, the resulting perturbation of the 1D model will need to be convected from the surface of the propellant to the exit of the 1D gas domain. Thus, if we inject in the CFD domain the fluxes that exit the 1D gas phase, the result of the input perturbation will be injected after a delay on the order of L/u_s, with u_s the 1D gas flow velocity at the surface. An arbitrary and non-physical delay results.

Ad hoc corrections can be thought of, e.g. injecting in the CFD domain the fluxes obtained at a dynamically calculated flame height x'_f in the 1D domain, for instance the point of highest temperature (x'_f in Fig. 7). However, conservativity of the coupling is lost, because these fluxes are not equal to those that exit the 1D domain. Also there remains a delay on the order of x'_f/u_s, which may still be erroneous.

This problematic would not occur if the 1D domain only extended up to the center of the first CFD cell above the surface. Then, direct connection between both domains could be possible by imposing the CFD state in that cell as the state at the end of the last 1D gas cell. However, with fine meshes required for an accurate computation of the conjugate heat transfer (on the order of 1 μm), the propellant flame would not be complete within the 1D domain, and would therefore need to be solved within the CFD solver as well, adding further complexities and computational cost to the overall coupled framework.

An alternative is to enforce the quasi-steadiness of the 1D gas phase. Thus, the gas phase instantaneously adapts itself to the variations of the input provided by the CFD solver, without any artificial delay. Conservativity is ensured by injecting in the CFD domain the fluxes that exit the 1D domain. The downside of this approach is the loss of dynamic effects resulting from the unsteady character of the 1D flame, however little is known experimentally about its effects.

The quasi-steady gas phase model thus corresponds to the classical QSHOD assumption (Quasi-Steady Homogeneous One-Dimensional) used for studying the response of the propellant to pressure oscillations. This is also in line with the previous ignition models from ONERA [16], where the gas flame is also assumed quasi-steady, but modelled in a simpler manner that allows for an analytical solution to be derived. From a mathematical point of view, the whole gas phase system (11)–(13) becomes algebraic of index-1, hence the specific time schemes presented in Section III.A.2 are still appropriate.

Note that, before ignition, the surface mass fractions of the reactants are negligible, thus no reaction occur and the

whole gas phase is uniform, with a temperature, composition and mass flow rate equal to those found at the surface.

B. Transition of the wall heat flux during ignition

Another non-trivial aspect is the formulation of the wall heat flux Φ_p that is transmitted by the CFD solver to the propellant solver. The wall heat flux is formulated in a similar fashion to a heat exchange law:

$$\Phi_w = \left(\lambda \partial_\eta T\right)_{\eta=0^+} = h(T_1 - T_w) \tag{17}$$

where T_w is the parietal temperature prescribed by the propellant solver, and T_1 is the gas temperature at the center of the first CFD cell above the propellant surface. The heat exchange coefficient is $h = \lambda/(\delta/2)$, with δ the height of the first CFD cell above the surface point considered. Thus, this expression constitutes a first-order finite difference approximation of the heat flux above the surface. For coarser meshes, wall laws could be used to improve the precision of this formula.

A propellant boundary face of the CFD domain successively goes through the following stages: inert heating, ignition, established burning. Let us analyse each of these phases to see how they affect the wall heat flux formulation.

1. Inert heating

When the propellant is not ignited, it behaves as an inert wall which is heated up the convective heat flux coming from the gas flow over its surface. Following Eq. (16), the resulting heat flux is imposed directly at the surface of the solid propellant from Vulc1D (see Fig. 7), thus bypassing the 1D gas phase, which may seem surprising at first. In our case, this gas phase is anyway enforced to behave in a quasi-steady manner, hence, before ignition, all the fields from the 1D gas phase are uniform and equal to their values at the surface, for instance $T = T_s$ across the whole 1D gas domain. It does not have any effect on that initial heating period, in particular the 1D flame model does not take heat away from the propellant surface via heat diffusion. That effect is captured by the coupling between the surface and fluid models, as is visible in Fig. 2. Following these remarks, it makes sense to set $T_w = T_s$ for the computation of the wall heat flux.

2. Established burning

Once the propellant is ignited, we assume that the 1D propellant flame completely isolates the propelllant from the surrounding flow. The only influence that CHARME can exert on Vulc1D is through the pressure P.

3. Ignition

Between the two previous phases, ignition occurs. During that short period, the solid propellant transitions from an inert material to an unsteady burning material with a large injected mass flow rate. Hence, there is also a transition that occurs in terms of conjugate heat-transfer. After ignition, the convective formulation heat transfer is not physically acceptable any more, as the propellant flame is expected to be the sole source of thermal energy for the propellant, as described in the previous paragraph. Therefore it is reasonable to formulate the wall heat flux such that it becomes zero at this stage.

Using the inert heating formulation:

$$\Phi_w = h(T_1 - T_s) \tag{18}$$

after ignition results in a very large "fictive" heat flux that greatly enhances the propellant consumption and should therefore be discarded. Moreover this post-ignition wall heat flux is proportional to $(T_1 - T_s)/\delta \approx (T_f - T_s)/\delta$, hence it diverges as the mesh is refined.

Another approach is to take the 1D flame temperature as the wall temperature T_w:

$$\Phi_w = h(T_1 - T_f) \tag{19}$$

with T_f the flame temperature (exit temperature from the 1D gas phase). The underlying idea is that $T_f = T_s$ during the inert heating period, and that T_1 tends to T_f once ignition as occurred, thus the heat flux will gradually decrease during ignition. Still, the heat flux ends up being slightly negative during established burning, but, more importantly, during the ignition period T_f will rise very rapidly, much more quickly than T_1. Consequently Φ_w will end up being very large and negative, causing an artificial slowdown of the ignition. In addition, this cooling flux also diverges as the mesh is refined, hence it is not acceptable.

A first correction could be to drive the wall heat flux to 0 by multiplying it by a sigmoid:

$$\Phi_w = h(T_1 - T_s)\,\sigma(T_f) \tag{20}$$

For example the sigmoid can be such that for $T_f < 2300$K, Φ_w is unaltered, and for $T_f > 2700$K, Φ_w is zero, with a smooth transition between both points. The sigmoid could also be applied on m, the surface mass flux instead. Typically $\sigma(T_f) = 0.5\left(1 - \tanh(\frac{T_f - 2500}{100})\right)$. Still, this pragmatic approach is artificial and different choices of the transition parameters may influence the ignition dynamics.

An alternative is to choose the same smoothing factor as for the heat transfer coefficient obtained in steady-state boundary layers with parietal mass injection [31], where the heat flux is multiplied by a decreasing exponential of the mass flow rate. This approach does however not seem suitable for the highly unsteady ignition event which we aim at simulating. Moreover, this correction assumes that the boundary layer above the propellant (which is a reactive layer in reality) behaves similarly to a conventional inert boundary layer with transpiration, which can be reasonably questioned.

In the present paper, we introduce and use the following hybrid formulation:

$$\Phi_w = \min\left(\max\left[\min\left(h(T_1 - T_s), h(T_1 - T_f)\right), 0\right], h(T_1 - T_s)\right) \tag{21}$$

Thus, the heat flux is coherent during inert heating, and is smoothly driven to zero following the increase of T_f during ignition. Additionally the wall heat flux can only be negative is $T_f = T_s$, i.e. if ignition has not yet occurred. This can be the case if an unignited propellant boundary face is suddenly exposed to a colder flow.

To our knowledge, all other ignition models from the literature behave like switches. The transition between an inert heating behaviour and a quasi-steady burning is instantaneous, typically upon reaching a predefined ignition temperature. Hence, the critical ignition interval where the propellant transitions from inert heating to established burning does not appear in these simulations.

Acknowledgments

The present research was conducted thanks to a Ph.D grant co-funded by DGA, Ministry of Defence (E. Faucher, Technical Advisor), and ONERA. The authors would like to thank Lionel Matuszewski and Philippe Grenard for their technical advice regarding the numerical developments.

References

[1] Parker, K., and Summerfield, M., "The ignition transient in solid propellant rocket motors," *Solid Propellant Rocket Conference*, 1964.

[2] Desoto, S., and Friedman, H. A., "Flame spreading and ignition transients in solid grain propellants," *AIAA Journal*, Vol. 3, No. 3, 1965, pp. 405–412.

[3] Peretz, A., Kuo, K. K., Caveny, L. H., and Summerfield, M., "Starting Transient of Solid-Propellant ocket Motors with High Internal Gas Velocities," *AIAA Journal*, Vol. 11, No. 12, 1973, pp. 1719–1727.

[4] d'Agostino, L., Biagioni, L., and Lamberti, G., "An Ignition Transient Model for Solid Propellant Rocket Motors," *37th Joint Propulsion Conference and Exhibit*, 2001.

[5] Johnston, W. A., "Solid rocket motor internal flow during ignition," *Journal of Propulsion and Power*, Vol. 11, No. 3, 1995, pp. 489–496.

[6] Alavilli, P., Buckmaster, J., Jackson, T., and Short, M., "Ignition-transient modeling for solid propellant rocket motors," *36th AIAA/ASME/SAE/ASSE Joint Propulsion Conference and Exhibit*, 2000.

[7] Koren, C., Vicquelin, R., and Gicquel, O., "Self-adaptive coupling frequency for unsteady coupled conjugate heat transfer simulations," *International Journal of Thermal Sciences*, Vol. 118, 2017, pp. 340 – 354.

[8] Radenac, E., Gressier, J., and Millan, P., "Methodology of numerical coupling for transient conjugate heat transfer," *Computers and Fluids*, Vol. 100, 2014, pp. 95 – 107.

[9] Erikson, W., and Beckstead, M., "Modeling unsteady monopropellant combustion with full chemical kinetics," *36th AIAA Aerospace Sciences Meeting and Exhibit*, 1998.

[10] Meredith, K., Gross, M., and Beckstead, M., "Laser-induced ignition modeling of HMX," *Comb. and Flame*, Vol. 162, 2014.

[11] Gallier, S., Ferrand, A., and Plaud, M., "Three-dimensional simulations of ignition of composite solid propellants," *Combustion and Flame*, Vol. 173, 2016, pp. 2–15.

[12] Meynet, N., "Simulation numérique de la combustion d'un propergol solide," Ph.D. thesis, Université Pierre et Marie Curie, 2005.

[13] Brandyberry, M., Fiedler, R., and McLay, C., "Verification and Validation of the Rocstar 3-D Multi-physics Solid Rocket Motor Simulation Program," *41st AIAA/ASME/SAE/ASSE Joint Propulsion Conference and Exhibit*, 2005.

[14] Li, Q., Liu, P., and He, G., "Fluid–solid coupled simulation of the ignition transient of solid rocket motor," *Acta Astronautica*, Vol. 110, 2015, pp. 180 – 190. Dynamics and Control of Space Systems.

[15] Li, Y., Chen, X., Xu, J., Zhou, C., and Musa, O., "Three-dimensional multi-physics coupled simulation of ignition transient in a dual pulse solid rocket motor," *Acta Astronautica*, Vol. 146, 2018, pp. 46–65.

[16] Bizot, A., "Ignition and Unsteady Combustion of AP-based Composite Propellants in Subscale Solid Rocket Motors," *International Journal of Energetic Materials and Chemical Propulsion*, Vol. 4, No. 1-6, 1997, pp. 1046–1061.

[17] Helley, P. L., "3D turbulent Navier Stokes simulations of ignition transients in solid rocket motors," *34th AIAA/ASME/SAE/ASSE Joint Propulsion Conference and Exhibit*, 1998.

[18] Orlandi, O., Fourmeaux, F., and Dupays, J., "Ignition Study at Small-Scale Solid Rocket Motor," *8th European Conference for Aeronautics and Space Sciences (EUCASS)*, 2019.

[19] François, L., Dupays, J., Davidenko, D., and Massot, M., "Travelling wave mathematical analysis and efficient numerical resolution for a one-dimensional model of solid propellant combustion," *Combustion Theory and Modelling*, Vol. 24, No. 5, 2020, pp. 775–809.

[20] François, L., Dupays, J., Davidenko, D., and Massot, M., "Solid propellant combustion in the low Mach one-dimensional approximation: from an index-one differential-algebraic formulation to high-fidelity simulations through high-order time integration with adaptive time-stepping," , arXiv:2007.02538.

[21] Refloch, A., Courbet, B., Murrone, A., Villedieu, P., Laurent, C., Gilbank, P., Troyes, J., Tessé, L., Chaineray, G., Dargaud, J.-B., Quémerais, E., and Vuillot, F., "CEDRE Software," *AerospaceLab Journal*, 2011, pp. 1–10.

[22] Menter, F., "Two-equation eddy-viscosity turbulence models for engineering applications," *AIAA Journal*, Vol. 32, 1994, pp. 1598–1605.

[23] Giovangigli, V., Meynet, N., and Smooke, M., "Application of continuation techniques to ammonium perchlorate plane flames," *Combustion Theory and Modelling*, Vol. 10, No. 5, 2006, pp. 771–798.

[24] Smith, D., "Modeling Solid Propellant Ignition Events," Ph.D. thesis, Brigham Young University, 2011.

[25] Le Touze, C., "Couplage entre modèles diphasiques à « phases séparées » et à « phase dispersée » pour la simulation de l'atomisation primaire en combustion cryotechnique," Ph.D. thesis, Université Nice Sophia Antipolis, 2015.

[26] Kværnø, A., "Singly Diagonally Implicit Runge–Kutta Methods with an Explicit First Stage," *BIT*, Vol. 44, 2004, pp. 489–502.

[27] François, L., "Multiphysical modelling and simulation of solid rocket motor ignition," Ph.D. thesis, Institut Polytechnique de Paris, 2022.

[28] François, L., Dupays, J., and Massot, M., "High-order adaptive coupling with error control for the simulation of solid rocket motor ignition," in preparation, 2021.

[29] Tseng, I., and Yang, V., "Combustion of a double-base homogeneous propellant in a rocket motor," *Combustion and Flame*, Vol. 96, No. 4, 1994, pp. 325–342.

[30] Dick, W., Fiedler, R., and Heath, M., "Building Rocstar: Simulation Science for Solid Propellant Rocket Motors," *42nd AIAA/ASME/SAE/ASSE Joint Propulsion Conference and Exhibit*, 2006.

[31] Bizot, A., "Turbulent boundary layer with mass transfer and pressure gradient in solid propellant rocket motors," *31st Joint Propulsion Conference and Exhibit*, 1995.